THE TROPICAL CYCLONE DIURNAL CYCLE IN CM1 USING AN ENSEMBLE APPROACH

Sarah Dunn Ditchek*, John Molinari, Robert G. Fovell, and Kristen L. Corbosiero

University at Albany, State University of New York, Albany, NY

1. INTRODUCTION

The tropical cyclone diurnal cycle (TCDC) manifests in different variables, for which consistent timing is found in the literature (Fig. 1): enhanced convection occurs overnight producing the coldest cloud-tops at around 4 LT; precipitation peaks at around 6 LT; and, starting at around 6 LT, the cirrus canopy expands radially outward and reaches its maximum areal extent at around 18 LT.

Despite the consistent timing found, there are conflicting theories behind what drives the cirrus canopy oscillation. To diagnose the underlying dynamics behind the observed TCDC and, in particular, the cirrus canopy, this research uses George Bryan's Cloud Model 1 (CM1; Bryan and Fritsch 2002; Bryan and Rotunno 2009) to create a "control run" which robustly reproduces the TCDC seen in observations. This control run will be used to study various cirrus canopy oscillation and inner-core convection hypotheses. The importance of the cirrus canopy to the TCDC will then be tested through sensitivity experiments involving cloud-radiative forcing (CRF).

2. METHODS

2.1 CM1 Model Setup

This study uses version 18.3 of CM1 in its axisymmetric mode, initialized with the tropical cyclone vortex and sounding from Rotunno and Emanuel (1987). The model is run for 12 days beginning on 8 August at 0000 LT on an f plane at 20 N and 0 W. Sea surface temperature is fixed at 26.13°C. The domain size is 3016 km wide and 25 km deep. Horizontal grid spacing is a uniform 2 km out to 500 km, after which the grid resolution is gradually stretched from 2 km to 15 km by the edge of the domain. Vertical grid spacing is gradually stretched from 40 m to 100 m from the lowest height level to 7 km and is then a uniform 100 m to the model top. A time step of 5 s is used, and output is saved every ten minutes. The NASA-Goddard radiation scheme (Chou and Suarez 1994, 1999) is called every five minutes. Thompson microphysics is used (Thompson et al. 2008), which in CM1 is single-moment in vapor, cloud, snow, and graupel, and is double-moment in rain and ice.

2.2 Extracting the Diurnal Harmonic

Fourier harmonic analysis is applied by fitting a series of sines and cosines to the data through least squares regression analysis. To understand the diurnal harmonic importance, the percentage of the total variance it explains is calculated. Additionally, the statistical significance is tested by taking the

* *Corresponding author address:* Sarah Dunn Ditchek, Univ. at Albany, Dept. of Atmospheric and Environmental Sciences, Albany, NY 12222; e-mail: sditchek@albany.edu.

ratio of the variance explained to the variance not explained by the diurnal harmonic and comparing that ratio to the F-value of the F-distribution at the 95% confidence level.

3. CREATING THE CONTROL RUN

A simulation that reproduces the observed TCDC is generated and tested for robustness. Here, the robustness of the modeled TCDC is assessed by taking an ensemble modeling approach and comparing the timing and magnitude of the resulting diurnal harmonic to observations found in Fig. 1.

To create the ensembles, a random Gaussian noise distribution with a mean of zero and a standard deviation of ten percent is applied to the surface latent and sensible heat fields at the initial time only. This process is performed five times to create a suite of ensemble members, each member being a manifestation of a slightly different storm. The suite is then averaged together over days when the storm is steady-state (days 6-12) to create an ensemble mean storm. Steady-state is defined as in Rogers et al. (2013): the 24-h moving difference field is within $\pm$ 5 m s^{-1}.

4. RESULTS

Results in this presentation focus on two vertically averaged layers: $\bar{z}$=10-14 km (the outflow layer) and $\bar{z}$=0-2 km (the inflow layer).

Both radial outflow aloft and inflow below peak at around 3-6 LT near the RMW (Fig. 2), consistent with the timing deep convection in the inner core seen in Fig. 1.

There is a column-deep signature of a diurnal cycle of storm size and intensity change (Fig. 3). At r$\geq$ 100 km, the storm reaches its maximum areal extent between 16-18 LT. At r$\leq$ 50 km near the RMW, the diurnal harmonic peaks at around 6-8 LT with an amplitude of 3.5 m s^{-1}.

Figure 4 depicts total condensate (the sum of cloud, rain, graupel, snow, and cloud ice mixing ratios) and net heating (the potential temperature tendency due to the interaction of longwave and shortwave radiation with hydrometeors). Total condensate peaks between 3-6 LT, consistent with the timing of deep convection in Fig. 1. Net cooling peaks at around 0 LT, consistent with overnight destabilization that is associated with early morning deep convection (Hobgood 1986).

The cloud ice mixing ratio component of total condensate (Fig. 5) increases over the course of the day, peaking at around 15 LT, indicative of cirrus canopy thickening. While not directly indicative of cirrus canopy expansion, the timing is consistent with Fig. 1.

Rainfall rate (Fig. 6) is maximized at inner radii closest to the RMW. Taking the $\bar{r}$=0-50 km area average, rainfall rate peaks at 5 LT, consistent with Fig. 1. Additionally, both the control run and Bowman and Fowler (2015) give a morning rainfall rate that is 15% larger than the evening rainfall rate.

5. CONCLUSION & FUTURE WORK

A robust control run of the TCDC has been produced. Its similarity to observations (Fig. 1) now allows for a deeper analysis to further understand the underlying dynamics behind the TCDC as portrayed by CM1. First, the control run will be analyzed and compared to various cirrus canopy oscillation and inner-core convection hypotheses. Then, CRF sensitivity experiments will be run related to the importance of the cirrus canopy to the TCDC.

6. ACKNOWLEDGEMENTS

7. REFERENCES

Bowman, K. P., and M. D. Fowler, 2015: The diurnal cycle of precipitation in tropical cyclones. J. Climate, 28 (13), 5325–5334.

Browner, S. P., W. L. Woodley, and C. G. Griffith, 1977: Diurnal oscillation of the area of cloudiness associated with tropical storms. Mon. Wea. Rev., 105 (7), 856–864.

Bryan, G. H., and J. M. Fritsch, 2002: A benchmark simulation for moist nonhydrostatic numerical models. Mon. Wea. Rev., 130 (12), 2917–2928.

Bryan, G. H., and R. Rotunno, 2009: The maximum intensity of tropical cyclones in axisymmetric numerical model simulations. Mon. Wea. Rev., 137 (6), 1770–1789.

Chou, M.-D., and M. J. Suarez, 1994: An efficient thermal infrared radiation parameterization for use in general circulation models. NASA Tech. Memo, 104606 (3), 85.

Chou, M.-D., and M. J. Suarez, 1999: A solar radiation parameterization for atmospheric studies. NASA Tech. Memo, 15, 40.

Dunion, J. P., C. D. Thorncroft, and C. S. Velden, 2014: The tropical cyclone diurnal cycle of mature hurricanes. Mon. Wea. Rev., 142 (10), 3900–3919.

Duran, P., and J. Molinari, 2016: Upper-tropospheric low Richardson number in tropical cyclones: Sensitivity to cyclone intensity and the diurnal cycle. J. Atmos. Sci., 73 (2), 545–554.

Frank,W. M., 1977: The structure and energetics of the tropical cyclone i. storm structure. Mon. Wea. Rev., 105 (9), 1119–1135.

Ge, X., Y. Ma, S. Zhou, and T. Li, 2014: Impacts of the diurnal cycle of radiation on tropical cyclone intensification and structure. Adv. Atmos. Sci., 31 (6), 1377–1385.

Hobgood, J. S., 1986: A possible mechanism for the diurnal oscillations of tropical cyclones. J. Atmos. Sci., 43 (23), 2901–2922.

Jiang, H., C. Liu, and E. J. Zipser, 2011: A TRMM-based tropical cyclone cloud and precipitation feature database. J. Appl. Meteor. Climatol., 50 (6), 1255–1274.

Kossin, J. P., 2002: Daily hurricane variability inferred from goes infrared imagery. Mon. Wea. Rev., 130 (9), 2260–2270.

Lajoie, F., and I. Butterworth, 1984: Oscillation of high-level cirrus and heavy precipitation around Australian region tropical cyclones. Mon. Wea. Rev., 112 (3), 535–544.

Leppert, K. D., and D. J. Cecil, 2016: Tropical cyclone diurnal cycle as observed by TRMM. Mon. Wea. Rev., 144 (8), 2793–2808.

Melhauser, C., and F. Zhang, 2014: Diurnal radiation cycle impact on the pregenesis environment of Hurricane Karl (2010). J. Atmos. Sci., 71 (4), 1241–1259.

Muramatsu, T., 1983: Diurnal variations of satellite-measured Tbb areal distribution and eye diameter of mature typhoons. J. Meteor. Soc. Japan, 61, 77–90.

Navarro, E. L., and G. J. Hakim, 2016: Idealized numerical modeling of the diurnal cycle of tropical cyclones. J. Atmos. Sci., 73 (10), 4189– 4201.

Navarro, E. L., G. J. Hakim, and H. E. Willoughby, 2017: Balanced response of an axisymmetric tropical cyclone to periodic diurnal heating. J. Atmos. Sci., 74 (10), 3325–3337.

Rogers, R., P. Reasor, and S. Lorsolo, 2013: Airborne Doppler observations of the inner-core structural differences between intensifying and steady-state tropical cyclones. Mon. Wea. Rev. 141 (9), 2970–2991.

Rotunno, R., and K. A. Emanuel, 1987: An air-sea interaction theory for tropical cyclones. Part II: Evolutionary study using a nonhydrostatic axisymmetric numerical model. J. Atmos. Sci., 44 (3), 542–561.

Shu, H.-L., Q.-H. Zhang, and B. Xu, 2013: Diurnal variation of tropical cyclone rainfall in the western North Pacific in 2008-2010. Atmos. Oceanic Sci. Lett., 6 (2), 103–108.

Smagorinsky, J., 1963: General circulation experiments with the primitive equations: I. the basic experiment. Mon. Wea. Rev., 91 (3), 99–164.

Steranka, J., E. B. Rodgers, and R. C. Gentry, 1984: The diurnal variation of Atlantic Ocean tropical cyclone cloud distribution inferred from geostationary satellite infrared measurements. Mon. Wea. Rev., 112 (11), 2338–2344.

Stevenson, S. N., K. L. Corbosiero, and S. F. Abarca, 2016: Lightning in eastern North Pacific tropical cyclones: A comparison to the North Atlantic. Mon. Wea. Rev., 144 (1), 225–239.

Thompson, G., P. R. Field, R. M. Rasmussen, and W. D. Hall, 2008: Explicit forecasts of winter precipitation using an improved bulk microphysics scheme. Part II: Implementation of a new snow parameterization. Mon. Wea. Rev., 136 (12), 5095–5115.

Wilhelmson, R. B., and C.-S. Chen, 1982: A simulation of the development of successive cells along a cold outflow boundary. J. Atmos. Sci., 39 (7), 1466–1483.

Wu, Q., and Z. Ruan, 2016: Diurnal variations of the areas and temperatures in tropical cyclone clouds. Quart. J. Roy. Meteor. Soc., 142 (700), 2788–2796.

Wu, Q., Z. Ruan, D. Chen, and T. Lian, 2015: Diurnal variations of tropical cyclone precipitation in the inner and outer rainbands. J. Geophys. Res., 120 (1), 1–11.

8. FIGURES
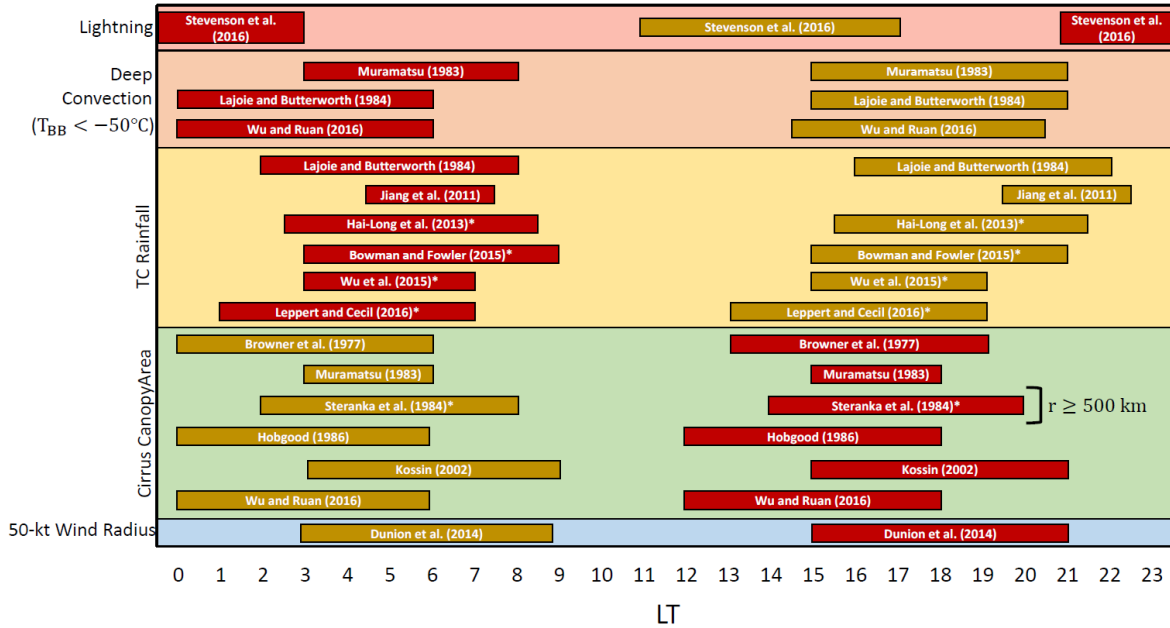
FIG. 1. A graphical view of results from papers on the TCDC. Papers are indicated by the author(s) and year of publication. The papers' findings regarding the timing of the TCDC are organized by local time (LT) on the x-axis. The maroon and gold boxes indicate the range of time when a variable's diurnal cycle is maximized or minimized, respectively. Variables are denoted along the y-axis, and each variable is associated with a different color block. An asterisk within a box indicates that a formal diurnal harmonic calculation was conducted in that study. In those cases, the width of the maroon and gold boxes corresponds to ± 3 hours of the maximum and minimum value of the diurnal harmonic for the given variable. If no asterisk is present, then the width of the boxes corresponds to the range of time associated with the diurnal cycle found in the text and figures of each paper.
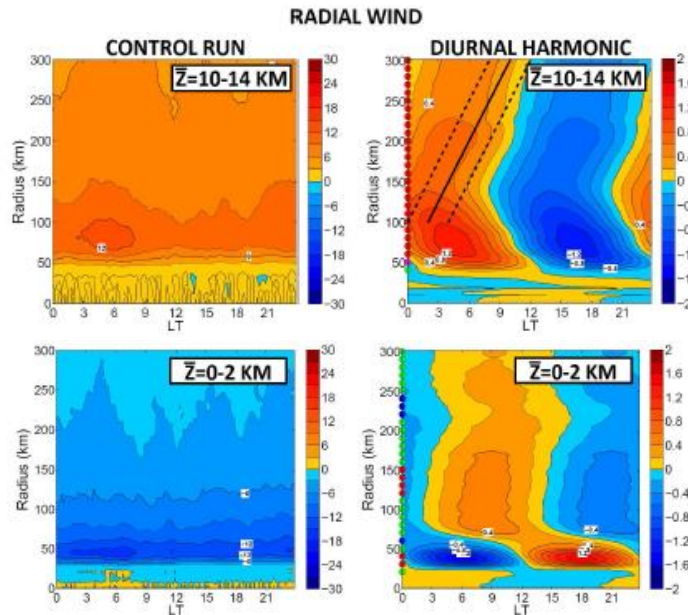
FIG. 2. The control run (column 1; contour interval, 3 m s^{-1}) and the corresponding diurnal harmonic (column 2; contour interval, 0.2 m s^{-1}) of radial wind. Dots along the y-axis in the diurnal harmonic plots indicate statistical significance of the diurnal harmonic at the 95% confidence level as determined by an F-test. The color of the dots indicate what range of variance is explained by the diurnal harmonic: blue for 0%–25%, green for 25%–50%, red for 50%–75%, and magenta for 75%–100%. Black lines correspond to the mean (solid), earliest, and latest (dashed) times of the onset of the Dunion et al. (2014) pulse.

3
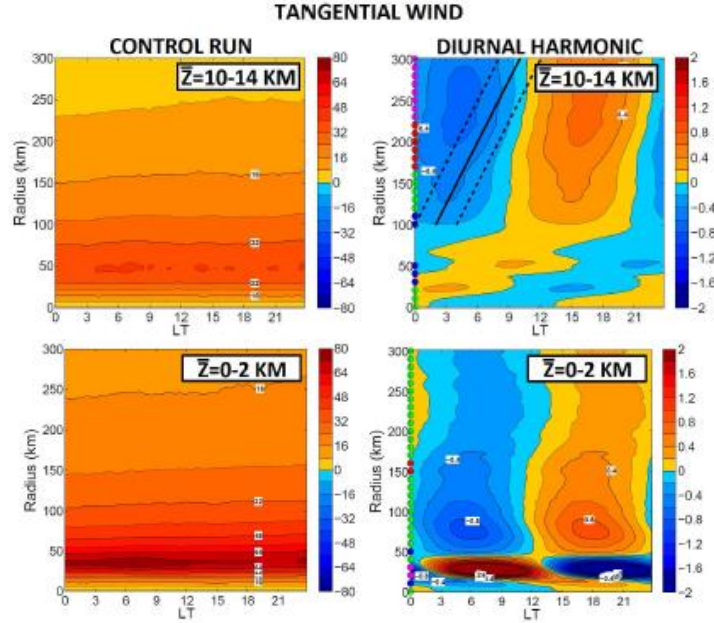
TANGENTIAL WIND

FIG. 3. The control run (column 1; contour interval, 8 m s⁻¹) and the corresponding diurnal harmonic (column 2; contour interval, 0.2 m s⁻¹) of tangential wind. The dots on the y-axis indicate statistical significance and explained variance as in Fig. 2. The solid and dashed lines indicate the Dunion et al. (2014) pulse as in Fig. 2.

TOTAL CONDENSATE & NET HEATING
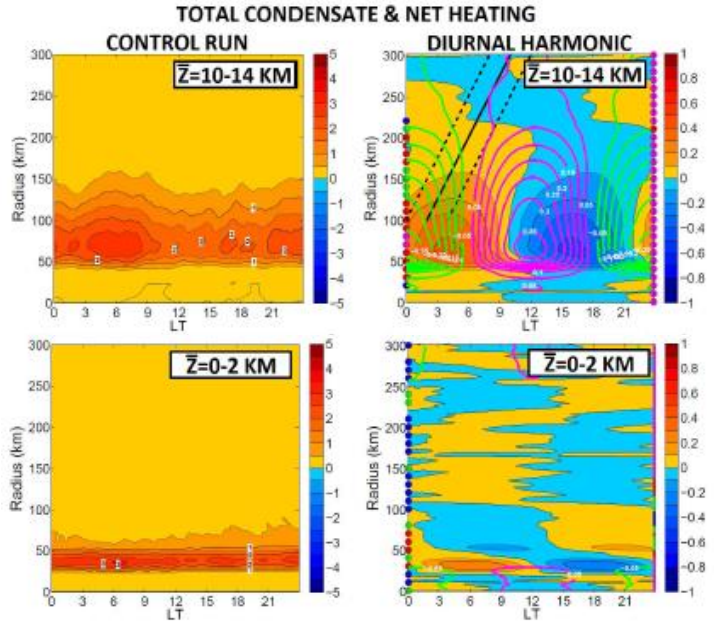
FIG. 4. The control run (column 1; contour interval, 0.5 g kg⁻¹) and the corresponding diurnal harmonic (column 2) of total condensate (contour interval, 0.1 g kg⁻¹) with overlaying contours of net shortwave and longwave heating (contour interval, 0.05 K hr⁻¹). The dots on the y-axis indicate statistical significance and explained variance as in Fig. 2. The solid and dashed lines indicate the Dunion et al. (2014) pulse as in Fig. 2.

4
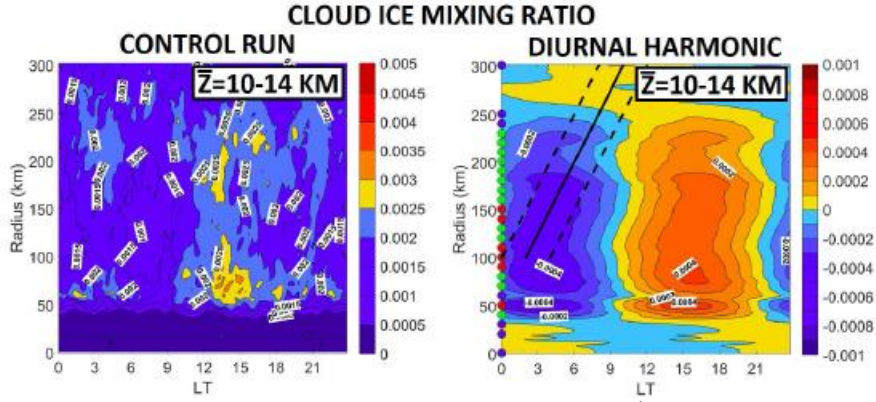
FIG. 5. The cloud ice mixing ratio of the control run (contour interval, 0.005 g kg^{-1}) and the corresponding diurnal harmonic (contour interval, 0.001 g kg^{-1}). The dots on the y-axis indicate statistical significance and explained variance as in Fig. 2. The solid and dashed lines indicate the Dunion et al. (2014) pulse as in Fig. 2.
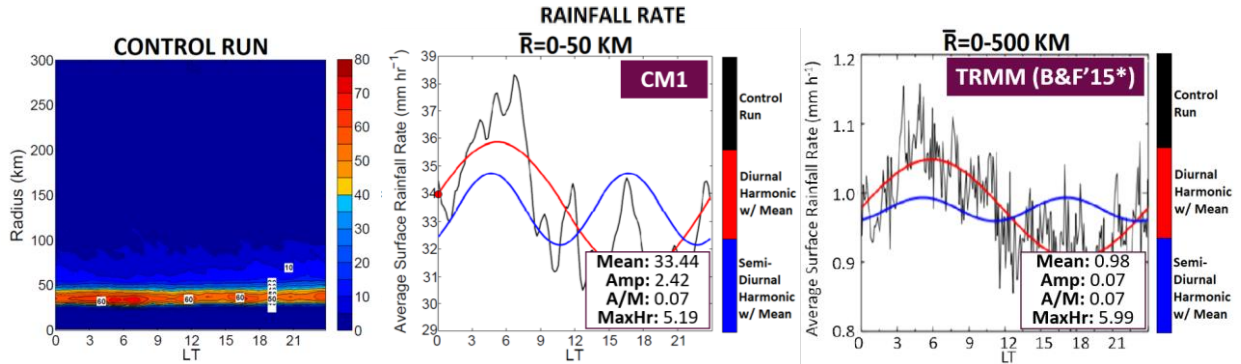
FIG. 6. The rainfall rate of the control run (contour interval, 5 mm hr^{-1}) and the radially averaged rainfall rate (black line), diurnal harmonic (red line), and semidiurnal harmonic (blue line) from the control run using CM1 ($\bar{r} = 0$–50 km) and Bowman and Fowler (2015) using TRMM ($\bar{r} = 0$–500 km). The dot on the y-axis indicates statistical significance and explained variance as in Fig. 2.

5